Unified Model of Disturbances Acting Upon Gimbal Seeker in Anti-Tank Guided Missile

Submitted: 7th October 2021; accepted: 9th February 2022

Radosław Nawrocki

DOI: 10.14313/JAMRIS/3-2021/19

Abstract:
Optimisation of the dynamic response of gimbal seeker plays key role from the point of view of development of anti-tank guided missile's systems. In this study the set of the most important internal disturbances were integrated in generalized model of two axis gimbal seeker implemented in MathWorks' Simulink environment. Compared to previous works on the subject, it was enhanced by replacing simple friction model with dynamic LuGre friction. Furthermore, its Coulomb component was linked to the normal force induced by missile's lateral acceleration. Control system of gimbal seeker proposed in paper was tuned with modelled disturbances turned off and then examined with them being turned one by one. System's responses were assessed to be significantly deteriorated, proving need of disturbance modelling and its use in control systems' design.

Keywords: *anti-tank guided missiles, gimbal seeker, disturbances, dynamic LuGre friction, imbalance, cross coupling*

1. Introduction

Third generation anti-tank guided missiles (ATGMs) are one of the most important development directions in category of precision-guided munitions. They owe this to their high effectiveness against armour achieved mostly by top attack capability and also user safety assured by fire and forget operation, despite their high price [1]. Their defining feature is gimbal seeker which, through means of tilting their line of sight, allows engaging targets from the top [2].

Third generation ATGMs, which are precise and highly integrated systems, are prone to many factors degrading their performance [3]. This is why it is especially important to identify and model disturbances acting upon them – mistakes made during their development phase are very costly.

Literature research shown significant number of papers concerning modelling gimbal seekers, taking into account not all, but some of possible disturbances. Aim of this paper is to evaluate current state of knowledge regarding disturbance modelling in context of gimbal seekers in third generation ATGMs, establish mathematical models for each disturbance and propose generalized disturbance model for such system.

2. Models of Individual Internal Disturbances in Gimbal Seeker

Main sources of disturbances were described in article by Masten [4]. By definition, some of them could be labelled as external, which means that their source is not directly associated with seeker, but rather its environment (vehicle motion, atmospheric disturbances [5, 6], etc.). Others are internal – inherently related to gimbal's physical phenomena and its structure. Most notable ones were listed below.

2.1. Friction

The most important goal of seeker's gimbal is to keep detector pointed towards acquired target or any other predefined fragment of space. Considering gimbal which uses direct drive to actuate its payload, it is easy to imagine that in idealized system with no friction, this goal would be achieved as a result of Newton's first law of motion [4]. No friction in bearings partially separates detector from missile movements that often could be stochastic in nature. Research by Lin, Hsiao [7] underlines how important coefficients of friction are in context of miss distance criterion, which is one of the most critical functional ATGM parameters. In this sense, miss distance can be defined as distance of missile's closest approach to target [8]. Fig. shows how increasing friction disturbance torque can quickly render missile useless, having in mind that commonly used HEAT warheads need direct hit to be effective, and standard NATO target used for evaluation of optical systems is 2.3 m × 2.3 m [9].

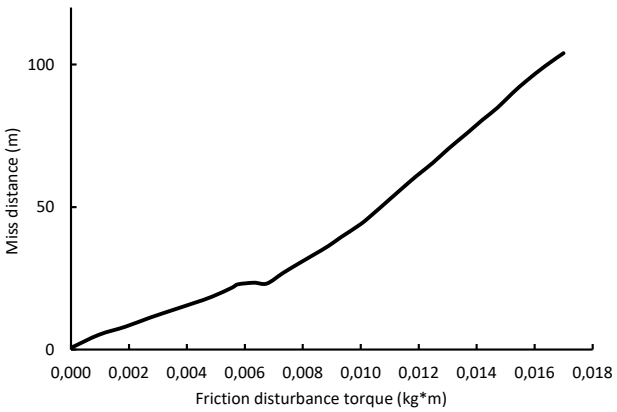

Fig. 1. Relationship between friction coefficient and miss distance [7]

According to Yu and Shang [3] system performance under heavy influence of disturbances could be improved either by enhancing control system parameters or minimizing their magnitude through refining mechanical system. That can be done by choosing right design solutions and improving quality of assembly process or even machining precision of single parts. Concerning friction, to alleviate its impact as a disturbance, ball bearings are commonly used to bear gimbal's structures mainly due to lower coefficients of friction.

Frictional component of torque disturbance could be modelled using many static and dynamic models as described in work of Olsson, Åström, Canudas de Wit, Gäfvert and Lischinsky [10]. Having in mind that in case of ATGM's gimbal one is dealing with highly dynamic movements with stops and changes of direction, only dynamic models seem to ensure sufficient level of detail to properly imitate physical behavior of such system. On top of that there are additional effects caused by bearing lubrication that should be addressed to fully model friction in gimbal bearings. The LuGre dynamic friction model was selected as one capturing many relevant friction aspects in missile gimbal's simulation.

As shown in paper by Dumitriu [11], LuGre friction model can be defined by set of three following equations.

$$\frac{dz}{dt} = v - \frac{\sigma_0 |v|}{g(v)} z \tag{1}$$

$$F = \sigma_0 z + \sigma_1 \dot{z} + \alpha_2 v \tag{2}$$

$$g(v) = F_C + (F_S - F_C) e^{-\left(\frac{v}{v_s}\right)^2} \tag{3}$$

where z stands for pre-sliding displacement, v for relative velocity of surfaces in friction, σ_0 for stiffness of the bristle, g(v) for function describing Stribeck's effect, F for friction force, σ_1 for damping, α_2 for viscous friction coefficient, F_C for Coulomb force, F_S for stiction force and v_s for Stribeck's velocity. Mentioned model could also be used to describe friction in bearings, but all linear parameters should be interpreted as angular (for example velocity v as angular velocity and force F as torque).

2.2. Gimbal Static Imbalance

Anti-tank guided missiles are often subjected to high accelerations following sudden movements of host vehicle induced by atmospheric disturbances or even intentional manoeuvres subsequent to deflection of missile's control surfaces [12]. Assuming that payload's centre of gravity (CG) is located exactly on azimuth and elevation gimbal's pivot axes, during acceleration there should not appear any additional torque. Any CG shift from that location generates disturbance torque directly proportional to payload's mass and offset distance. That effect is called gimbal's static imbalance. According to Toloei, Abdo, Vali and Arvan [13] those disturbance torques could be modelled as follows:

$$T_{S-EL} = m_{EL} a_m R_{EL} \cos(\theta_m + \varepsilon + \theta_{EL}) \tag{4}$$

$$T_{S-AZ} = m_{AZ} a_m R_{AZ} \cos(\Psi_m + \eta + \theta_{AZ}) \tag{5}$$

where T_{S-EL} and T_{S-AZ} stand for elevation and azimuth disturbance torque respectively, m_{EL} for mass of elevation gimbal, m_{AZ} for mass of azimuth gimbal, a_m for lateral missile acceleration, R_{EL} for centre of gravity (CG) offset distance to elevation gimbal's pivot axis, R_{AZ} for CG offset distance to azimuth gimbal's pivot axis, θ_m for missile body angle in vertical plane, Ψ_m for missile body angle in horizontal plane, ε for elevation gimbal angle, η for azimuth gimbal angle, θ_{EL} for gimbal offset elevation angle, θ_{AZ} for gimbal offset azimuth angle.

The problem with the equations presented herein is that proposed model does not concern a_m changing with missile rates caused by external disturbances as a result of Newton's second law of motion. Slight change was proposed and presented in equations (6) and (7).

$$T_{S-EL} = m_{EL} \left(\left(\frac{d\omega_{Pj}}{dt} \times R_{MG} \right) + g \right) R_{EL} \cos(\theta_m + \varepsilon + \theta_{EL}) \tag{6}$$

$$T_{S-AZ} = m_{AZ} \left(\frac{d\omega_{Pk}}{dt} \times R_{MG} \right) R_{AZ} \cos(\Psi_m + \eta + \theta_{AZ}) \tag{7}$$

where ω_{Pj} stands for missile pitch rate, R_{MG} for distance between missile's centre of gravity (CG) and gimbal's CG, g for standard acceleration due to gravity and ω_{Pk} for missile yaw rate. This way elevation and azimuth torque disturbances are dependent on missile movements, what closer resembles reality.

2.3. Gimbal Cross Coupling

Besides static imbalance, factual missile gimbal is characterized by dynamic imbalance which is caused by non-symmetrical mass distribution around its rotation axes. Said imbalance manifests itself by products of inertia and results in non-diagonal inertia matrix [13]. It is important to mention that even when gimbal is statically balanced it does not mean that it can't be dynamically imbalanced [12].

As can be seen in paper by Toloei, Abdo, Vali and Arvan [13], in equations of gimbal motion derived through use of Lagrange equation, there are disturbance torques in which described products of inertia occur. What's more, in azimuth's gimbal equations there are products of inertia and rates of elevation gimbal and that causes phenomenon called cross coupling where movement involving only one gimbal transfers to the other. For example, equation of motion for azimuth gimbal is formulated like this [13]:

$$J_{eq} \dot{\omega}_{Ad} = T_{Az} \cos(\varepsilon) + (T_{d1} + T_{d2} + T_{d3}) \cos(\varepsilon) + T_d' \tag{8}$$

where J_{eq} stands for instantaneous moment of inertia of azimuth gimbal around k axis, $\dot{\omega}_{Ad}$ for acceleration of gimbal's payload around d axis, T_{AZ} for azimuth gimbal's motor torque, ε for deflection of elevation gimbal and T_{d1}, T_{d2}, T_{d3}, T_d' for different components

of disturbance torque. Taking only last of them into consideration we get following equations [13].

$$T_d' = J_{eq}\left(\dot{\omega}_{Bn}\sin(\varepsilon) + \omega_{Ar}(\omega_{Ae} - \omega_{Be})\right) \quad (9)$$

$$J_{eq} = B_k + A_r\sin^2(\varepsilon) + A_d\cos^2(\varepsilon) - A_{rd}\sin(2\varepsilon) \quad (10)$$

where $\dot{\omega}_{Bn}$ stands for acceleration of azimuth gimbal around n axis, ω_{Ar} for elevation gimbal's rate around r axis, ω_{Ae} for elevation gimbal's rate around e axis, ω_{Be} for azimuth gimbal's rate around e axis, B_k for moment of inertia of azimuth gimbal around k axis, A_r for moment of inertia of elevation gimbal around r axis, A_d for moment of inertia of elevation gimbal around d axis, A_{rd} for elevation gimbal moment of inertia around r axis, when rotated around d axis (product of inertia).

As can be easily seen, parameters associated with elevation gimbal (rates and moments of inertia) cause additional azimuth gimbal's disturbance torque. As result of that every elevation gimbal movement have to be addressed by control system of other gimbal.

2.4. Cable Flexure

Being highly integrated electromechanical devices, gimbal seekers often require electrical connections between their payload and host vehicle. The only exception are systems employing steering stabilization paradigm, which move optical elements to manipulate line of sight (LOS) rather than whole sensor fixed to missile fuselage [4]. In classical configuration, where at least few of the connections such as video signal transmission are necessary, designer have to deal with periodically changing disturbance torque originating from cable flexure [14].

According to Wang [14] currently there is no well-established spring disturbance torque model that can be used during gimbal seeker design. Previous works focus mainly on models prepared for use in marine cable installation [15, 16]. Gimbal designers have to rely on building psychical models, often when rest of the design is already completed. Wang proposed and validated model based on Kirchhoff rod theorem, which proved to be well suited for this kind of task.

Due to model's complexity and need for precise formulation of cable harness mounting conditions, as it affects expected results, it was decided to leave cable flexure out of developed generalized model.

3. Proposed Generalized Model of Gimbal

Considering above internal disturbances, generalized model of two axis gimbal seeker was built using Simulink environment within MathWorks' MATLAB. Many previous works touched on subject of deriving two-axis gimbal's equations of motion [17-19]. Herein, structure is based on one introduced in paper by Toloei, Abdo, Vali and Arvan [13], although changes were made including: replacing simple friction model with dynamic LuGre friction model and also making it dependent upon missile's angular acceleration (Coulomb friction part of it). Also, separate subsystem for generating external missile pitch rate disturbance was highlighted. In table 1 all parameters used in model are listed with their corresponding symbols.

Tab. 1. Parameters and their symbols used in model

Parameter	Symbol	Comment
Input elevation rate command generated by tracking loop	ω_EL	–
Input azimuth rate command generated by tracking loop	ω_AZ	Assumed 0 – model was examined in pitch axis
Missile roll rate	ω_Pi	Assumed 0 – model was examined in pitch axis
Missile pitch rate	ω_Pj	–
Missile yaw rate	ω_Pk	Assumed 0 – model was examined in pitch axis
Elevation gimbal deflection	ε, epsilon	–
Azimuth gimbal deflection	η, eta	–
Elevation gimbal rate around d axis in relation to inertial frame	ω_Ad	–
Elevation gimbal rate around e axis in relation to inertial frame	ω_Ae	–
Elevation gimbal rate around r axis in relation to inertial frame	ω_Ar	–
Azimuth gimbal rate around k axis in relation to inertial frame	ω_Bk	–
Azimuth gimbal rate around e axis in relation to inertial frame	ω_Be	–
Azimuth gimbal rate around n axis in relation to inertial frame	ω_Bn	–
Elevation gimbal disturbance torque	T_D-EL	Result of cross coupling between azimuth and elevation gimbals

Parameter	Symbol	Comment
Azimuth gimbal disturbance torque	T_D-AZ	Result of cross coupling between azimuth and elevation gimbals
Instantaneous moment of inertia of azimuth gimbal around k axis	J_eq	Changes with deflection of elevation gimbal
Elevation gimbal moment of inertia around e axis	A_e	Assumed 0.1 kg × m^2
Elevation gimbal moment of inertia around r axis	A_r	Assumed 0.1 kg × m^2
Elevation gimbal moment of inertia around d axis	A_d	Assumed 0.1 kg × m^2
Azimuth gimbal moment of inertia around k axis	B_k	Assumed 0.1 kg × m^2
Azimuth gimbal moment of inertia around e axis	B_e	Assumed 0.1 kg × m^2
Azimuth gimbal moment of inertia around n axis	B_n	Assumed 0.1 kg × m^2
Elevation gimbal moment of inertia around r axis, when rotated around e axis (product of inertia)	A_re	Assumed 0.05 kg × m^2
Elevation gimbal moment of inertia around r axis, when rotated around d axis (product of inertia)	A_rd	Assumed 0.05 kg × m^2
Elevation gimbal moment of inertia around d axis, when rotated around e axis (product of inertia)	A_de	Assumed 0.05 kg × m^2
Azimuth gimbal moment of inertia around n axis, when rotated around e axis (product of inertia)	B_ne	Assumed 0.05 kg × m^2
Azimuth gimbal moment of inertia around n axis, when rotated around k axis (product of inertia)	B_nk	Assumed 0.05 kg × m^2
Azimuth gimbal moment of inertia around k axis, when rotated around e axis (product of inertia)	B_ke	Assumed 0.05 kg × m^2
Back EMF constant of the motor	K_e	Assumed $0.85\frac{\text{Vs}}{\text{rad}}$ as in [11]
Torque constant of the motor	K_TM	Assumed $0.85\frac{\text{Nm}}{\text{A}}$ as in [11]
Terminal inductance	L_a	Assumed 0.003 H as in [11]
Terminal resistance	R_a	Assumed 4.5 Ω as in [11]
Torque of the elevation gimbal's motor	T_EL	–
Torque of the azimuth gimbal's motor	T_AZ	–
Mass of elevation gimbal	m_EL	Assumed 0.4 kg
Mass of azimuth gimbal	m_AZ	Assumed 0.4 kg
Rate gyro natural frequency	ω_n	Assumed 50 Hz as in [11]
Azimuth gimbal CG offset distance from its rotation axis	R_AZ	Assumed 0.2 m as in [11]
Elevation gimbal CG offset distance from its rotation axis	R_EL	Assumed 0.2 m as in [11]
Gimbal offset distance from missile's CG	R_MG	Assumed 0.7 m
Gimbal offset elevation angle	Teta_EL	Assumed 0 as when gimbal axis in initial position is coaxial with missile body axis
Gimbal offset azimuth angle	Teta_AZ	Assumed 0 as when gimbal axis in initial position is coaxial with missile body axis
Rate gyro damping coefficient	ksi	Assumed 0.7 as in [11]
Missile vertical acceleration	a_el	–
Coefficient of rolling friction	mi	Assumed 0.005 m
LuGre bristle stiffness parameter	sigma0	Assumed $1000\frac{\text{Nm}}{\text{rad}}$

Parameter	Symbol	Comment
LuGre damping coefficient	sigma1	Assumed $2\frac{\text{Nm}\times\text{s}}{\text{rad}}$
LuGre stiction force with Coulomb friction subtracted	alfa1	Assumed 0.5 Nm
LuGre coefficient of viscous friction	alfa2	Assumed $0.01\frac{\text{Nm}\times\text{s}}{\text{rad}}$
Stribeck velocity	vs	Assumed $0.01\frac{\text{rad}}{\text{s}}$

In the following figures generalized model of gimbal is shown, starting with overview of whole system (figure 2), followed by close up of elevation and azimuth gimbal (figure 3 and 4 respectively). Next, cross coupling subsystem is shown with missile movement signal generator subsystem (figure 5). Inside of the first can be seen in figure 6 and 7. Figures 8 and 9 show static imbalance and LuGre dynamic friction subsystems.

In the model overview we can see outer part of the model consisting of two inner stabilization loops (rate control), cross coupling between them and also missile pitch rate disturbance generator subsystem. Output from each rate stabilization loops is used to close second, position tracking loop. For this purpose, PI controller is used. Reference value for azimuth tracking loop is set to zero because in this paper only elevation system's response is considered.

Closeup of elevation and azimuth gimbal disturbance rejection loops shown in figures 3 and 4 reveals their internal structure with DC motor, rate gyro, inertia block and summation node where all disturbances are added (static imbalance, friction, cross coupling disturbance). It's important to point out dependency between elevation and azimuth gimbal – elevation gimbal deflection ε acts as one of the inputs to azimuth gimbal subsystem and is used as a multiplier to motor's torque, azimuth gimbal's rates and also changes its inertia.

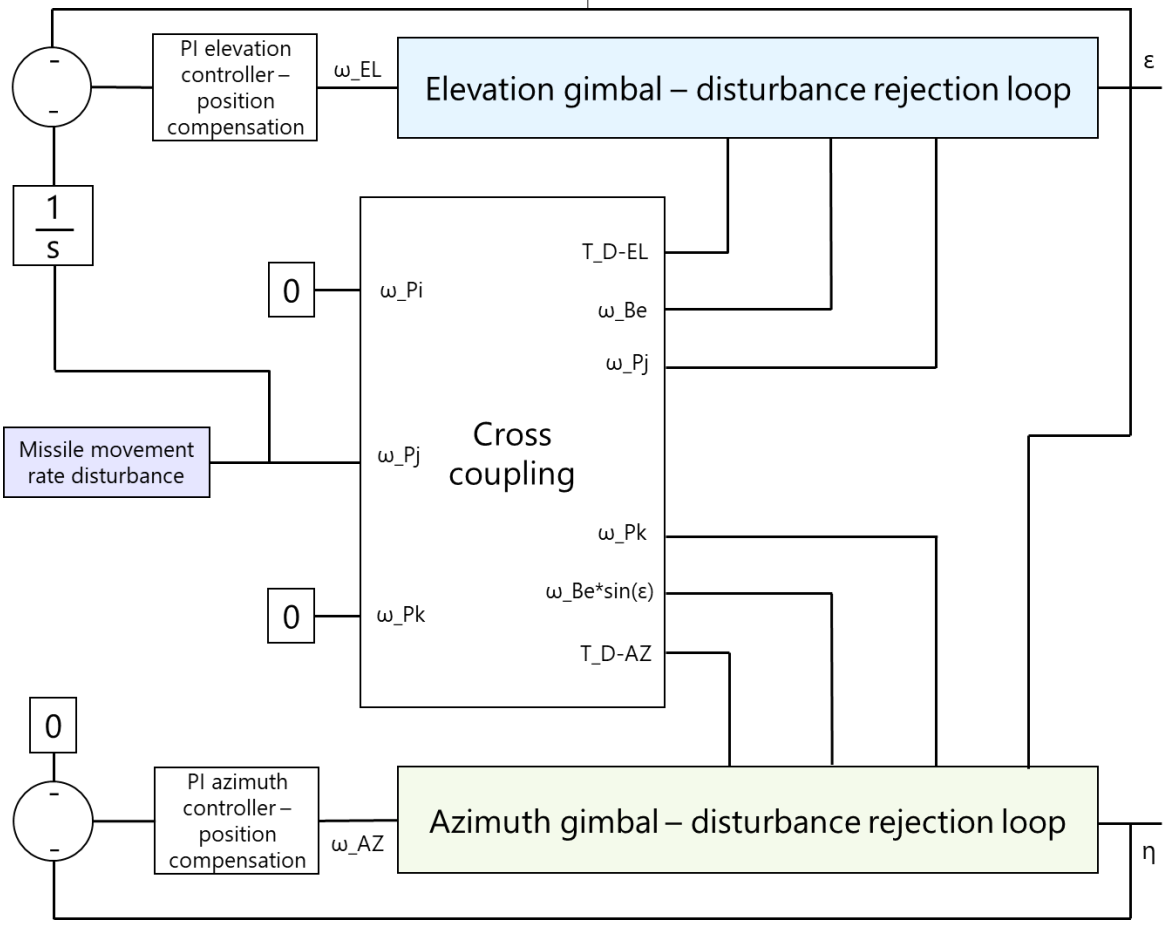

Fig. 2. Simplified overview of gimbal seeker model

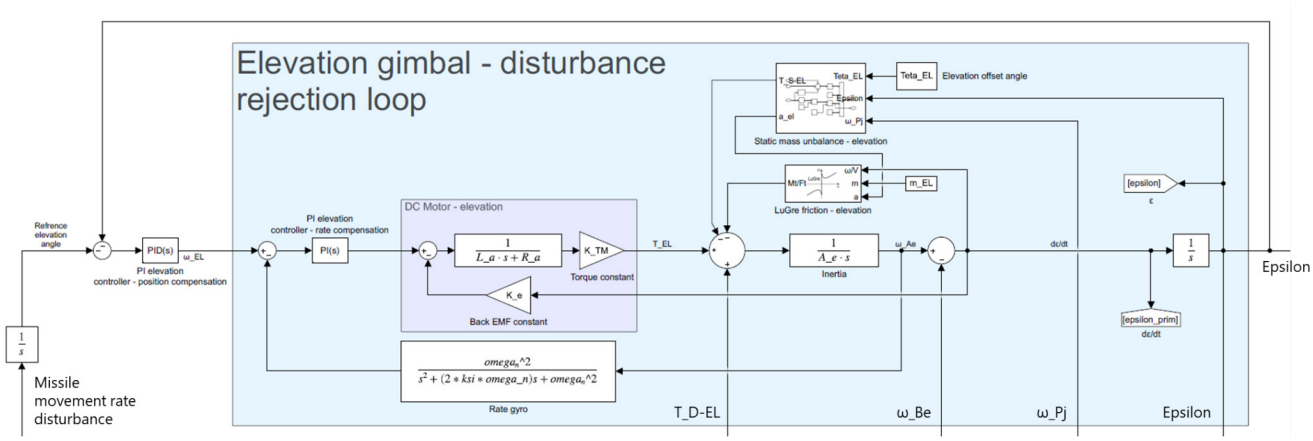

Fig. 3. Elevation gimbal control loops

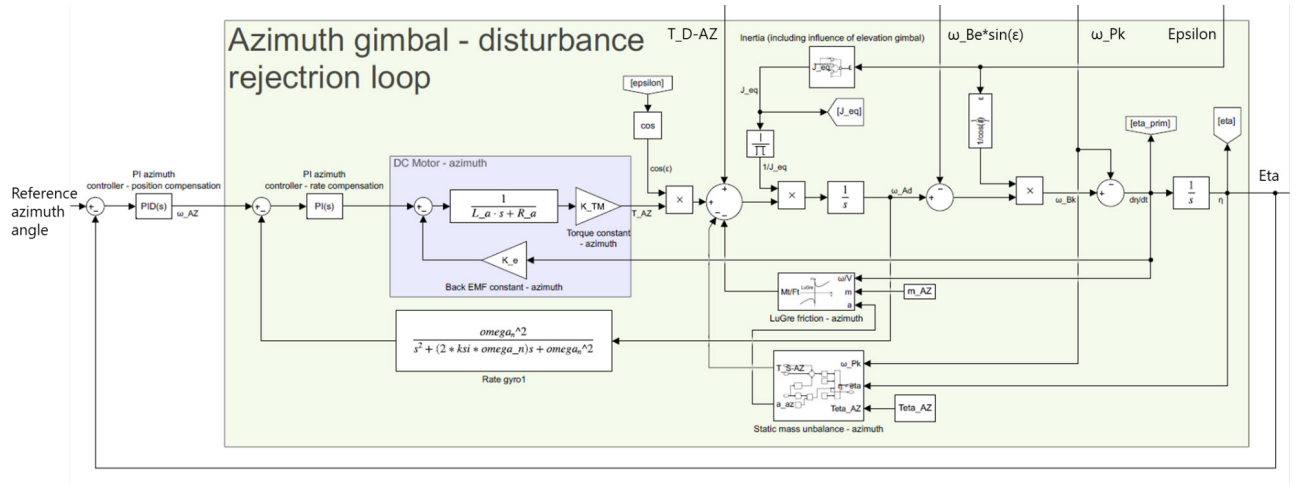

Fig. 4. Azimuth gimbal control loops

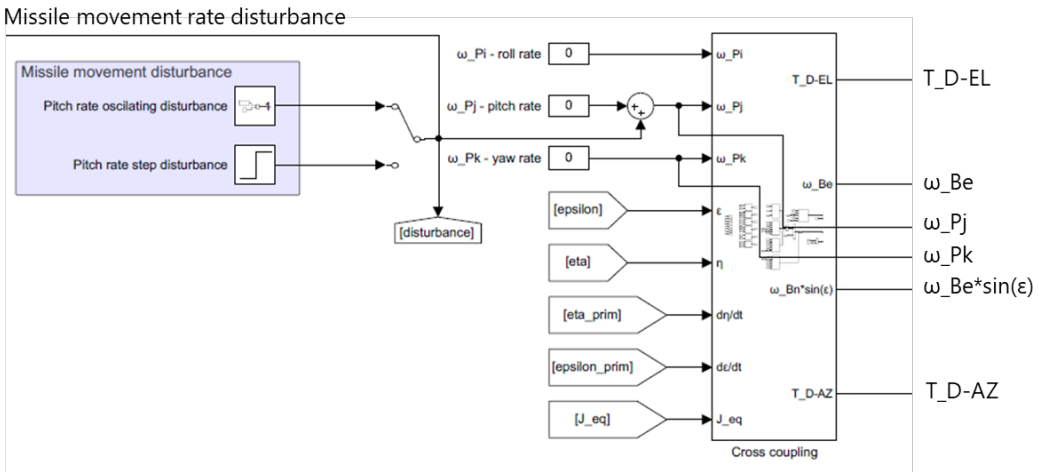

Fig. 5. Missile disturbance block and cross coupling between gimbals

As can be seen in figure 5 missile movement disturbance subsystem consists of step signal generator and oscillatory signal generator (to examine input signals used for tests see subsection 3.1). Inside of cross coupling subsystem is shown in the following figures. There are several MATLAB function blocks containing elevation and azimuth gimbal's rates calculations (figure 6) and cross coupling disturbance torques calculation (figure 7). Used equations are synonymous to those derived by Toloei, Abdo, Vali and Arvan [13] in their work.

Lateral acceleration of gimbal a_el is being extracted from static imbalance subsystem as can be seen in figure 8. It is later used to calculate alfa0 coefficient in LuGre dynamic friction model subsystem, which corresponds with a level of Coulomb friction. This way additional tension on bearings during high-G missile manoeuvres transfers to higher friction torques in said bearings. This nuance differentiates hereby paper from previous works of Toloei, Abdo, Vali and Arvan [13].

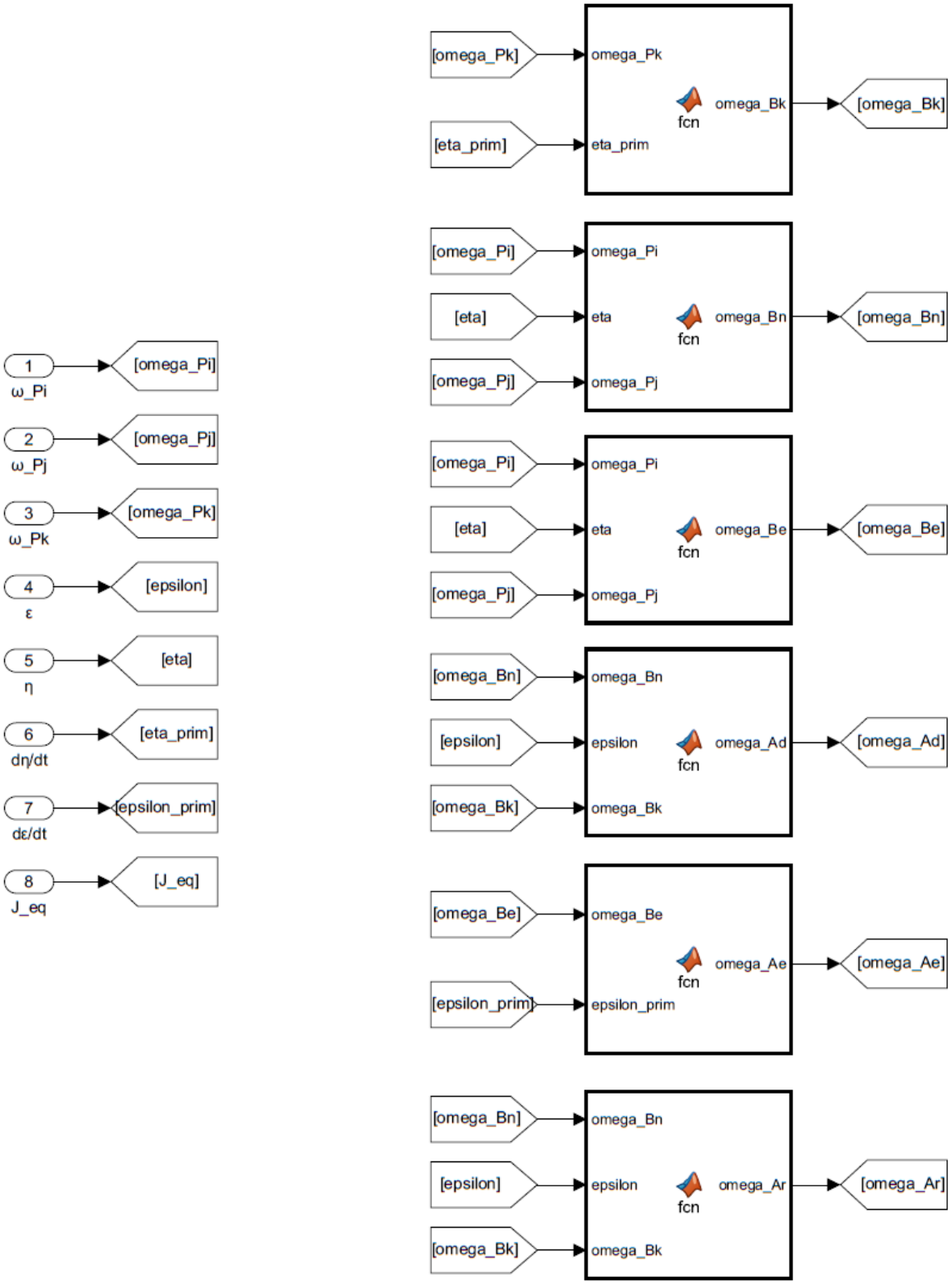

Fig. 6. Inside of cross coupling between elevation and azimuth gimbal subsystem – rates calculation

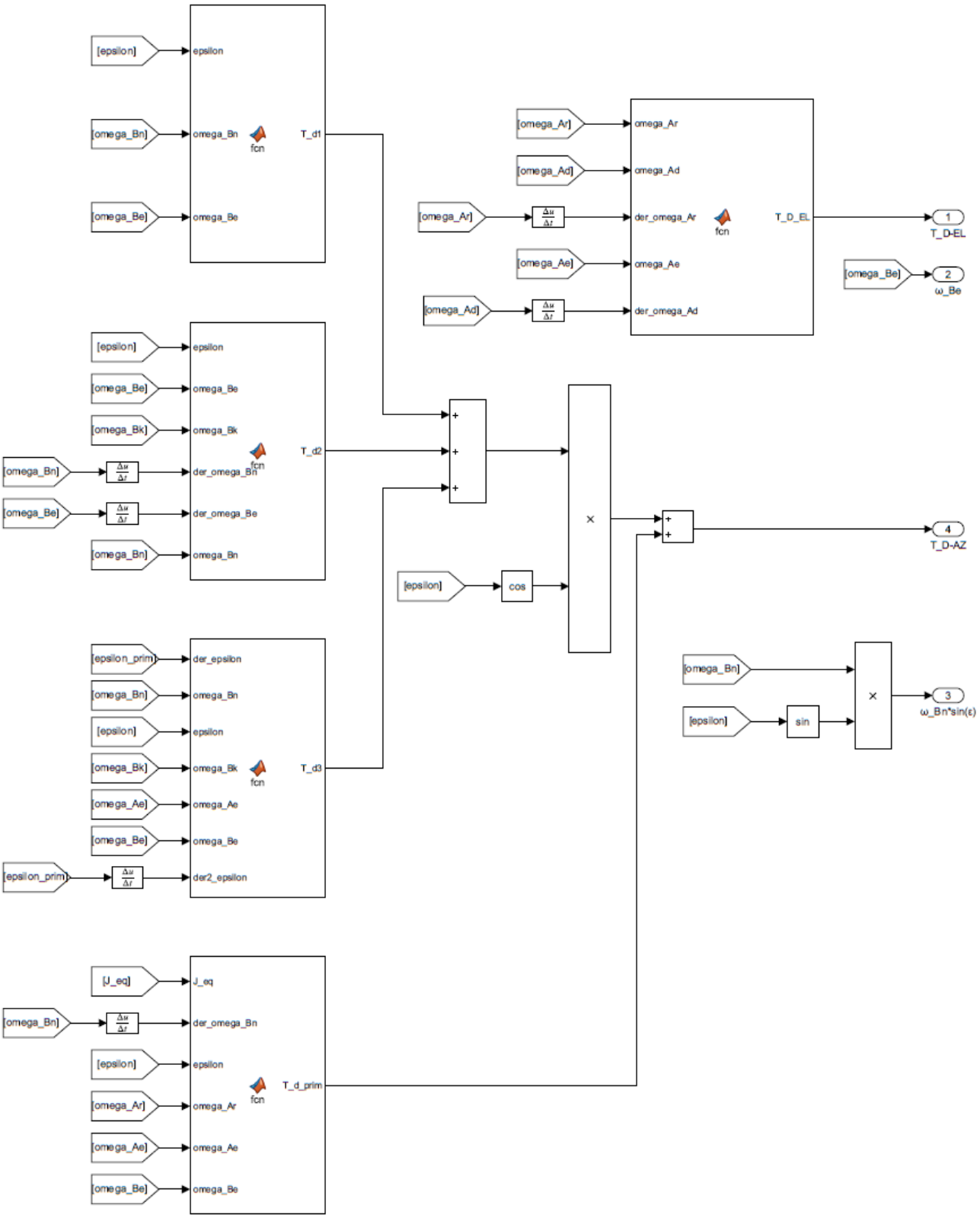

Fig. 7. Inside of cross coupling between elevation and azimuth gimbal subsystem – disturbance torques calculation

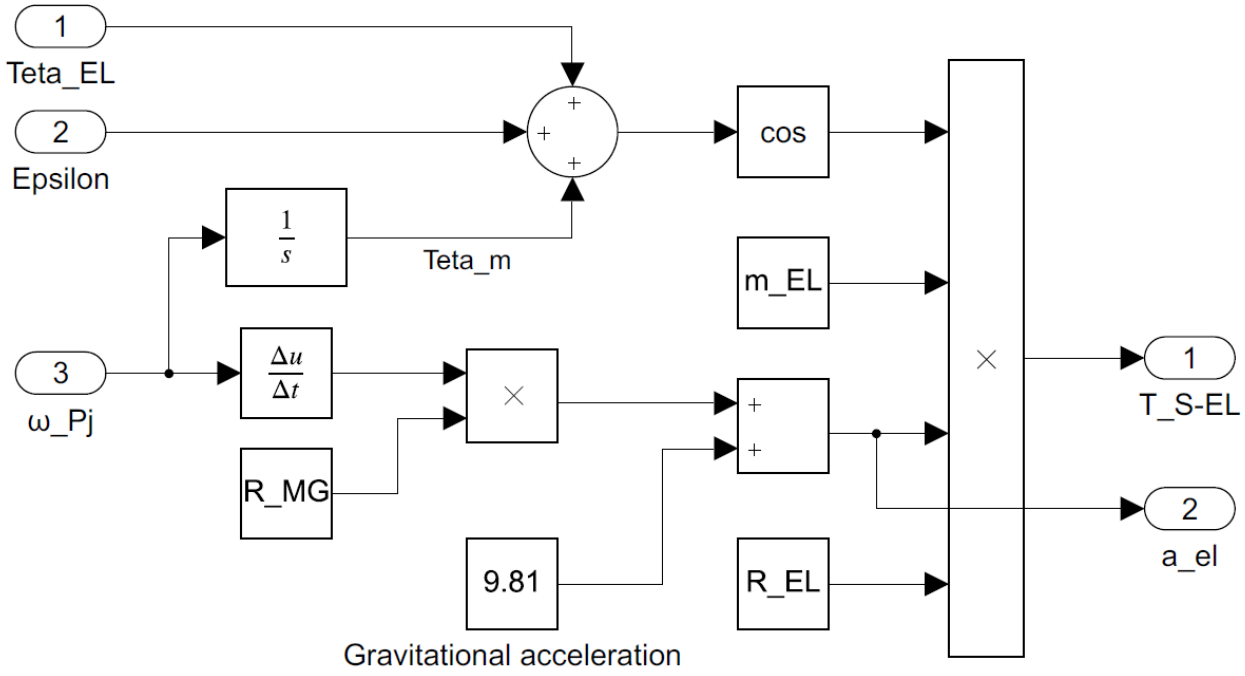

Fig. 8. Static imbalance subsystem for elevation gimbal

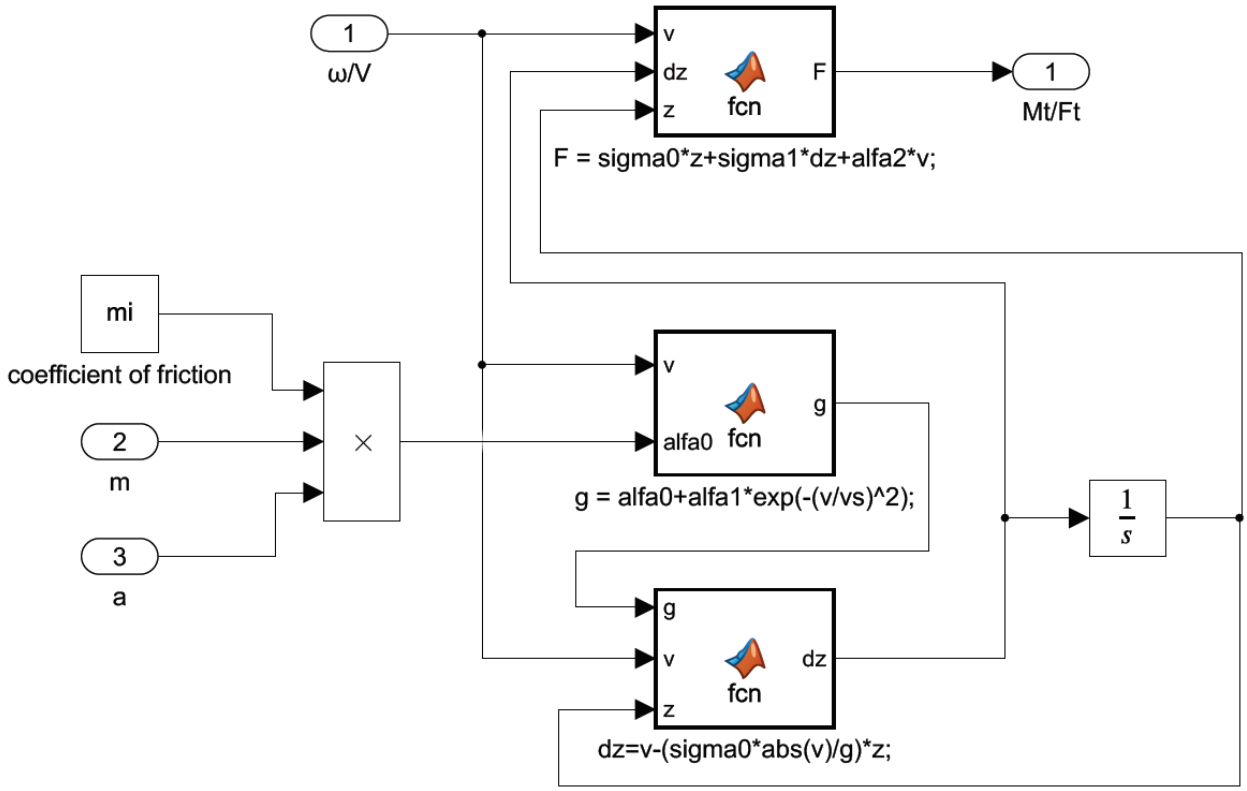

Fig. 9. LuGre dynamic friction model subsystem [11]

3. Results of Modelling

3.1. External Disturbances

To see how individual internal disturbances affect responses of modelled system, two missile pitch rate input signals were proposed. First one imitates situation where sudden gust of wind pushes missile out of its trajectory and then stops allowing it to restore its initial position (figure 10a; oscillations with decreasing amplitude). Second one is classic step input signal which corresponds to situation of going into very sudden missile turn and continuing it with steady rate (figure 10b).

First all internal disturbances (cross coupling disturbance torque, static imbalance and LuGre friction) had been disabled and then rate and position controllers were auto-tuned with Simulink's PID tuning app. Following figures show responses of system just to said external disturbances.

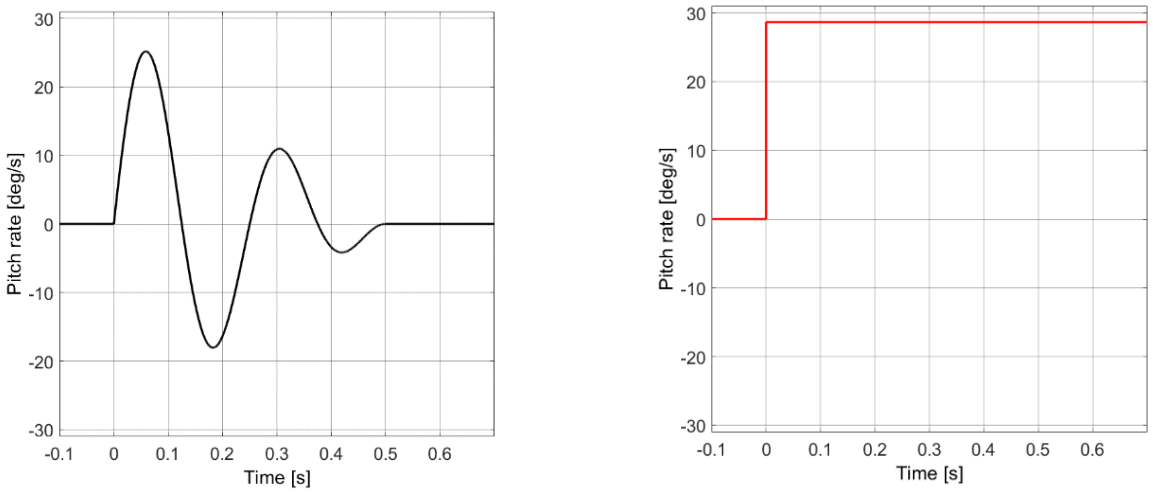

(a) (b)

Fig. 10. Missile pitch rate disturbances: oscillatory (a) and step (b) used to visualize influence of internal disturbances

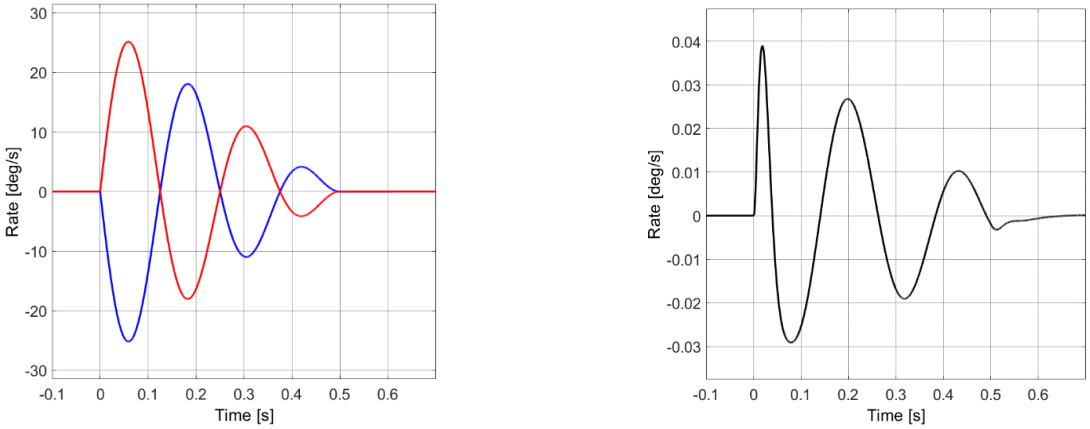

(a) (b)

Fig. 11. System response without additional internal disturbances: missile pitch rate oscillating disturbance (a, red plot), elevation gimbal rate response (a, blue plot) and line of sight (LOS) elevation rate (b, black plot)

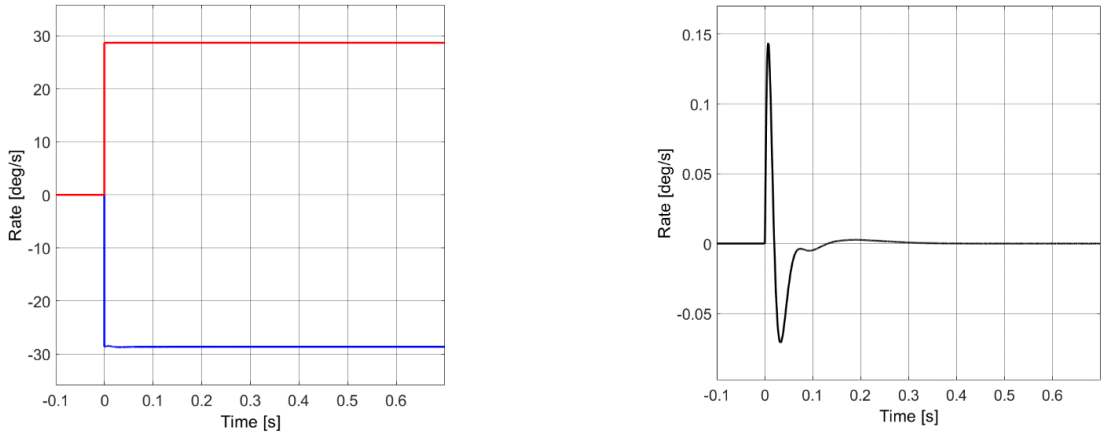

(a) (b)

Fig. 12. System response without additional internal disturbances: missile pitch rate step disturbance (a, red plot), elevation gimbal rate response (a, blue plot) and LOS elevation rate (b, black plot)

3.2. Effects of Implementing LuGre Friction Model

After initial tests without internal disturbances, LuGre friction subsystem was enabled. **What is important is that auto-tuned controllers settings set initially were left unchanged. This way we can assess disturbance rejection ability of the model and also evaluate if examined disturbance significantly affects system.** Following figures show system responses with LuGre friction included.

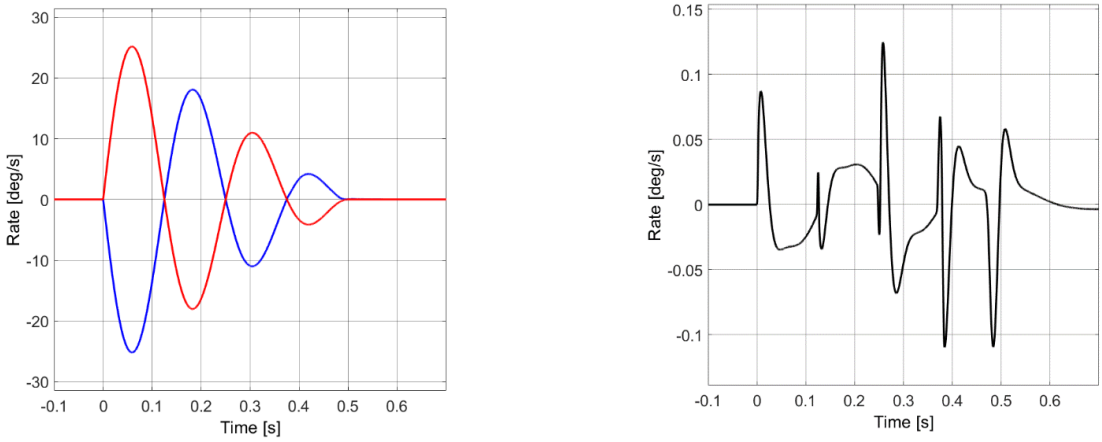

(a) (b)

Fig. 13. System response with LuGre friction: missile pitch rate oscillating disturbance (a, red plot), elevation gimbal rate response (a, blue plot) and LOS elevation rate (b, black plot)

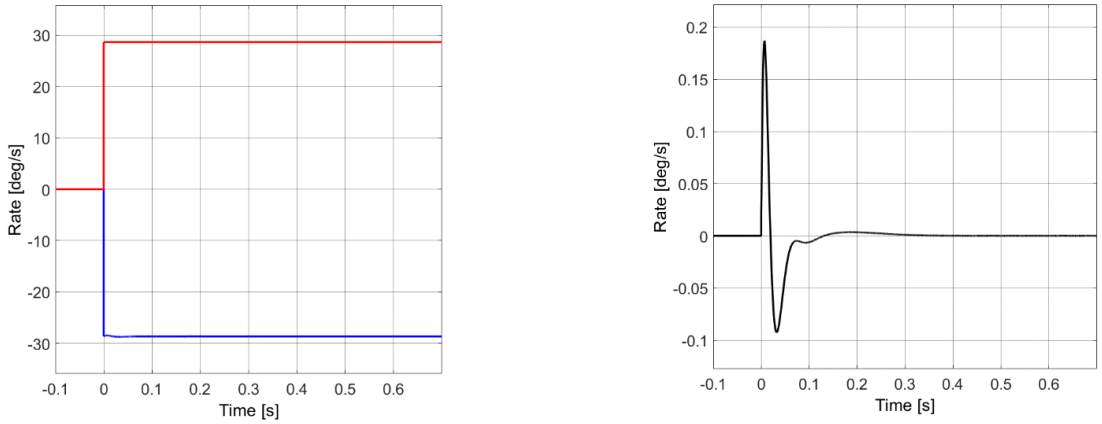

(a) (b)

Fig. 14. System response with LuGre friction: missile pitch rate step disturbance (a, red plot), elevation gimbal rate response (a, blue plot) and LOS elevation rate (b, black plot)

3.3. Effects of Implementing Static Imbalance Model

Next friction disturbance was substituted with static imbalance what led to system responses shown on following figures.

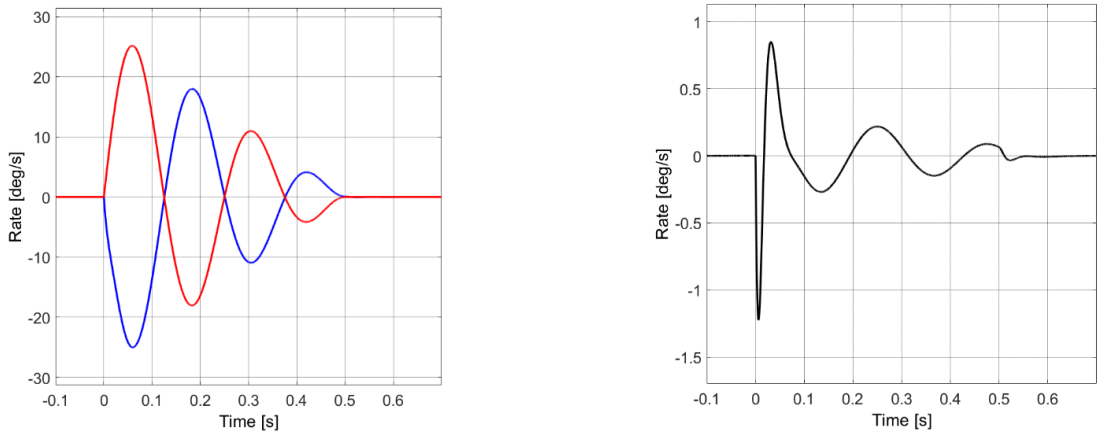

(a) (b)

Fig. 15. System response with static imbalance: missile pitch rate oscillating disturbance (a, red plot), elevation gimbal rate response (a, blue plot) and LOS elevation rate (b, black plot)

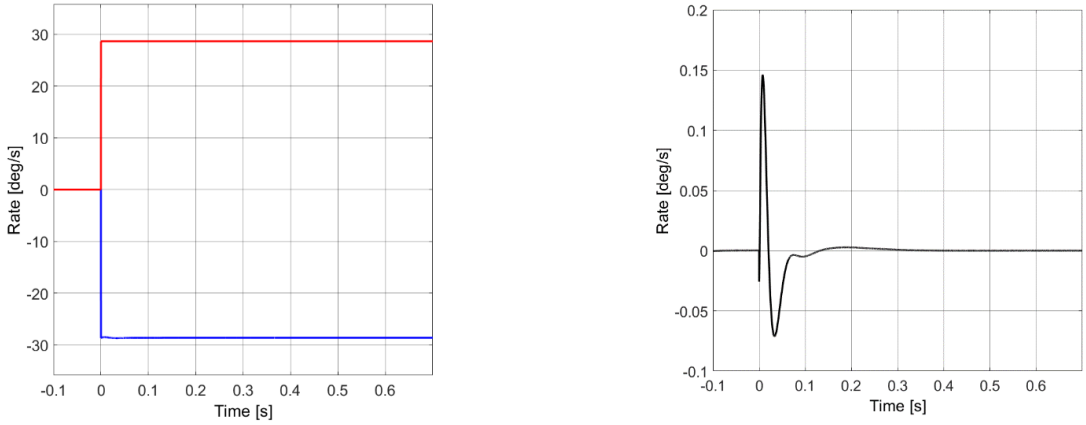

(a) (b)

Fig. 16. System response with static imbalance: missile pitch rate step disturbance (a, red plot), elevation gimbal rate response (a, blue plot) and LOS elevation rate (b, black plot)

3.3. Effects of Implementing Cross Coupling Model

Last internal disturbance to examine was that associated with cross coupling. Following figures show how it affects system response.

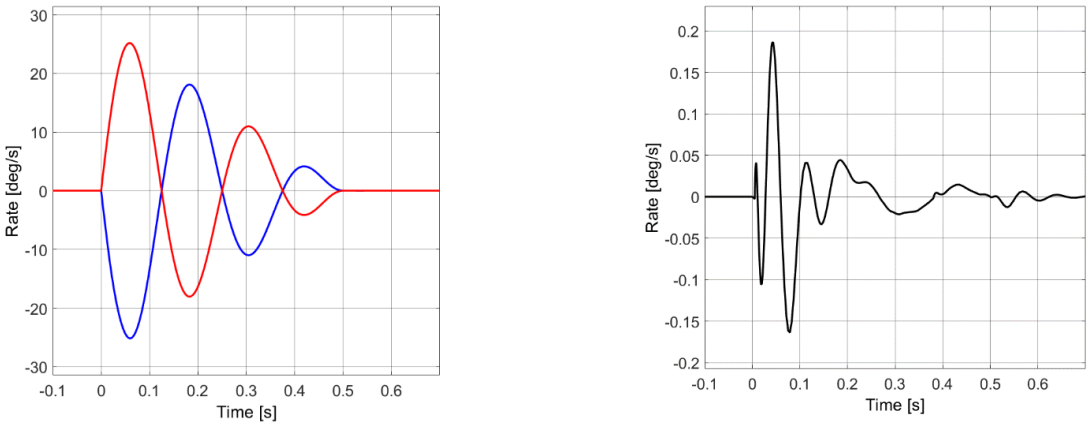

(a) (b)

Fig. 17. System response with cross coupling: missile pitch rate oscillating disturbance (a, red plot), elevation gimbal rate response (a, blue plot) and LOS elevation rate (b, black plot)

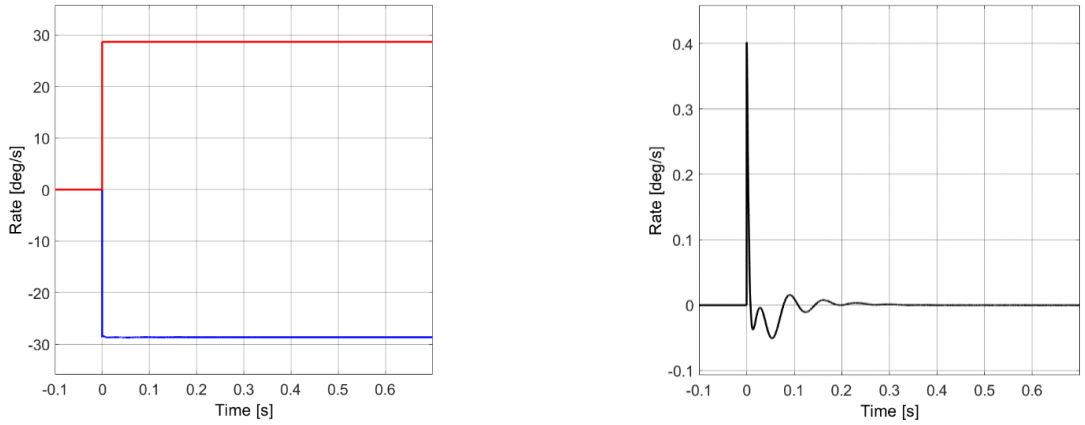

(a) (b)

Fig. 18. System response with cross coupling: missile pitch rate step disturbance (a, red plot), elevation gimbal rate response (a, blue plot) and LOS elevation rate (b, black plot)

Another important fact to consider is cross coupling's effect on gimbal's second axis which reveals itself when examining LOS azimuth rate during missile pitch rate disturbance. Following figures show side by side comparison of LOS elevation and azimuth rate.

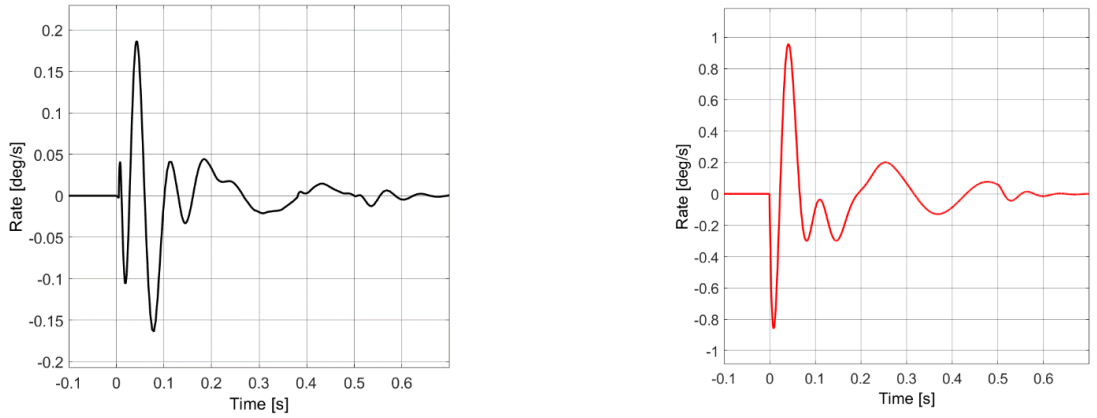

(a) (b)

Fig. 19. Azimuth gimbal response to elevation gimbal moving during missile pitch rate oscillating disturbance – LOS elevation rate (a) and azimuth rate (b)

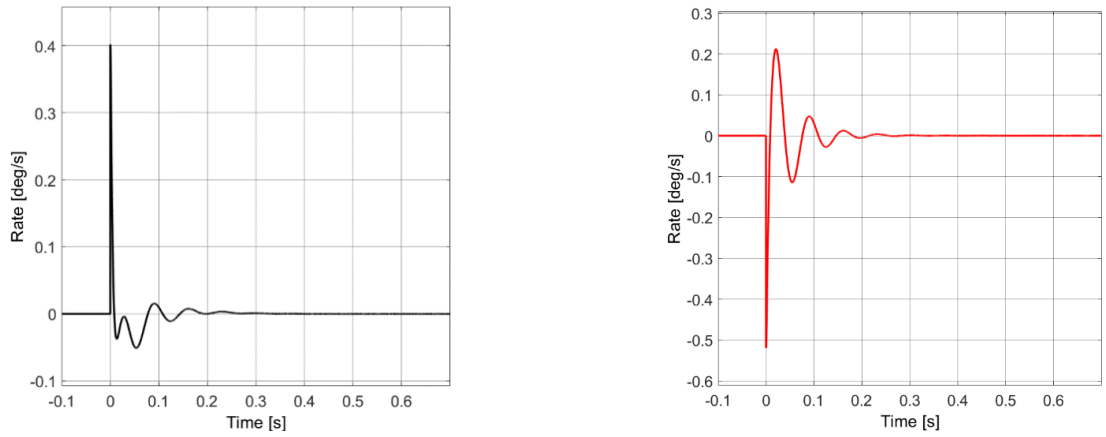

(a) (b)

Fig. 20. Azimuth gimbal response to elevation gimbal moving during missile pitch rate step disturbance – LOS elevation rate (a) and azimuth rate (b)

3.4. Generalized Model

Ultimately all internal disturbances were considered, as can be seen on model schematics in section 3 of hereby paper. An influence on system's response to this generalized internal disturbance model was shown in figures 21 and 22.

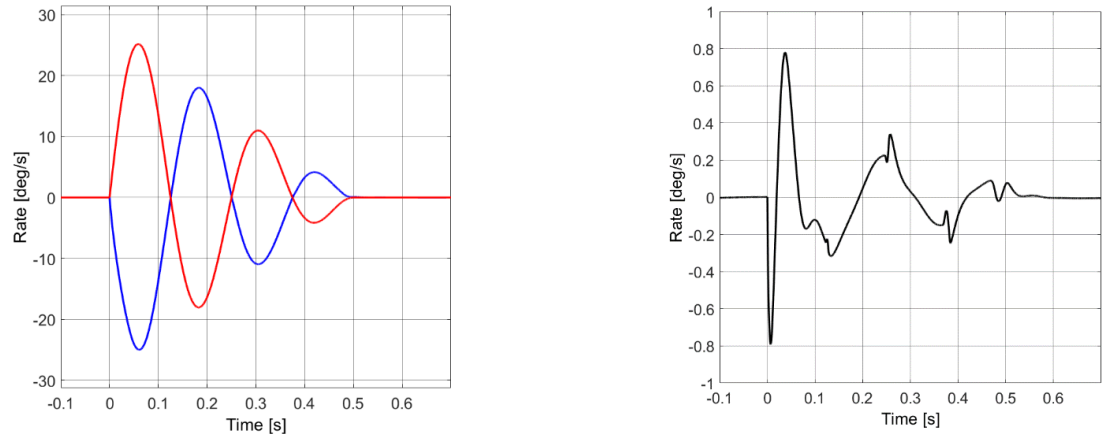

(a) (b)

Fig. 21. System response with all internal disturbances considered: missile pitch rate oscillating disturbance (a, red plot), elevation gimbal rate response (a, blue plot) and LOS elevation rate (b, black plot)

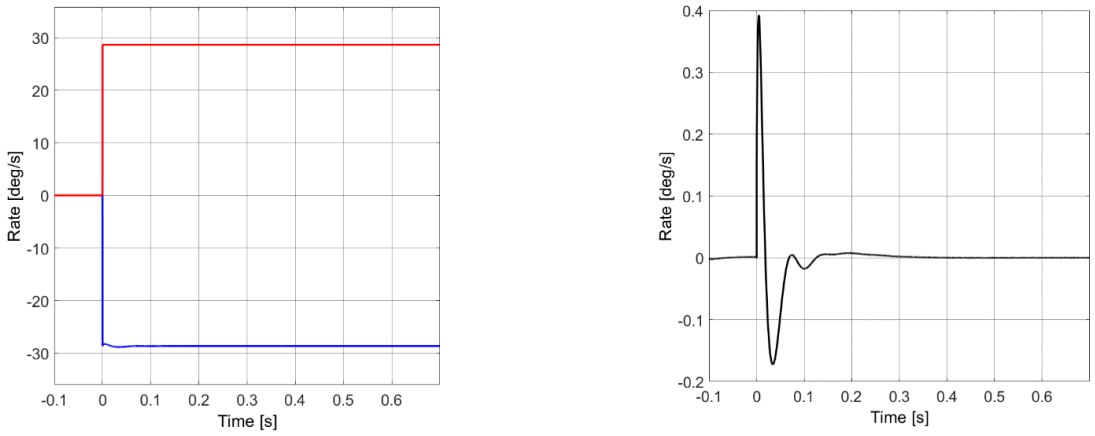

(a) (b)

Fig. 22. System response with all internal disturbances: missile pitch rate oscillating disturbance (a, red plot), elevation gimbal rate response (a, blue plot) and LOS elevation rate (b, black plot)

4. Discussion

As expected, while examining disturbances, system response turned out to be deteriorated in terms of LOS rate's peak amplitude and also change in regularity of plotted curves - each internal disturbance was assessed as significant.

LuGre friction made elevation LOS's peak rate almost double during oscillatory external disturbance and also introduced additional peaks with zero-velocity crossing of the gimbal. Supposedly this is due to stiction – an effect which is captured by LuGre friction model. Static imbalance doesn't necessarily change character of LOS rate's curve, but significantly increases its amplitude during oscillations of missile. With assumed parameters change was at least order of magnitude greater than without static imbalance. Lastly, cross coupling not only changed LOS rate of elevation gimbal in terms of amplitude and characteristic, but also induced additional disturbance torques in azimuth gimbal, which had to be addressed by control system to keep LOS still.

All internal disturbances combined seem to affect LOS elevation rate accordingly – with changes in amplitude and plot characteristic, but not necessarily generating worst responses. In fact, some of the disturbance's effects cancel out, so the amplitude peaks are not higher than when single disturbances were examined.

Gimbal's inner rate control loops, sometimes called stabilization loops, are meant to keep LOS stable during flight, so seeker would never lose track of acquired target. This can happen when LOS deflection from zero position (line perpendicular to detector's focal plane array connecting its centre with the target) surpasses system's field of view (FOV). So, the real functional parameters of gimbal seeker are not LOS rates like discussed before, but rather LOS deflections shown in figures 20 and 21.

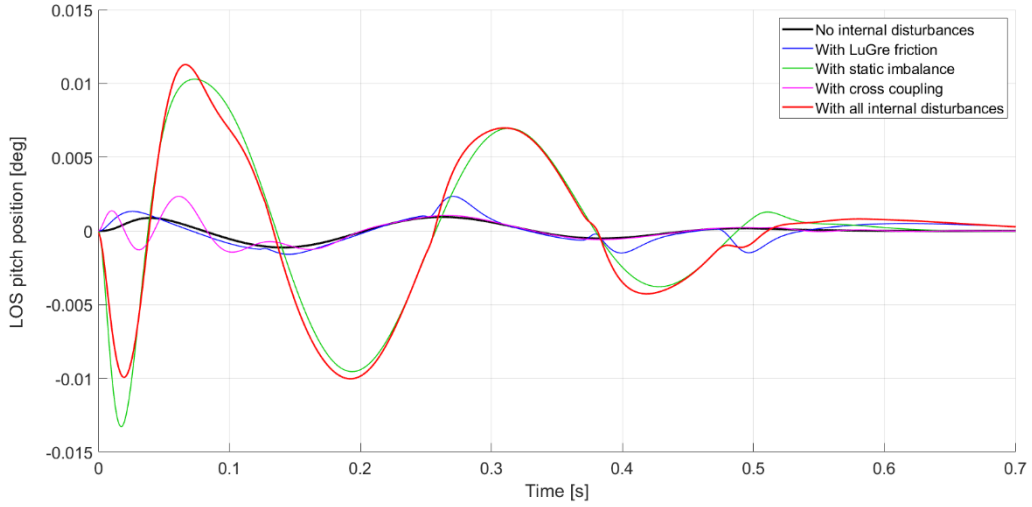

Fig. 23. LOS deflection in result of missile pitch oscillating disturbance and other modelled disturbances

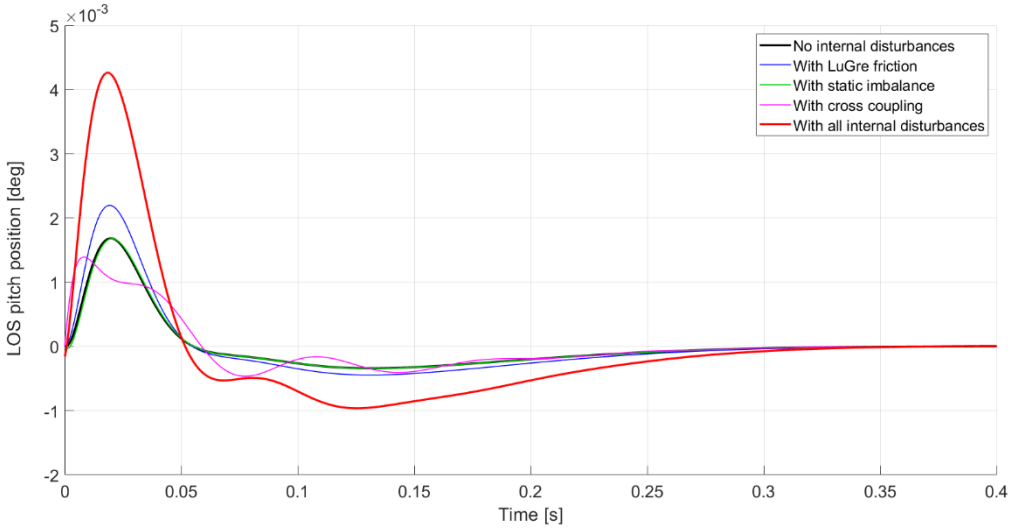

Fig. 24. LOS deflection in result of missile pitch step disturbance and other modelled disturbances

As can be seen in above figures, incorporating internal disturbance's models leads to degradation in functioning of gimbal's control system. Although shown characteristics (black – no internal disturbances and red – all internal disturbances) differ significantly, in terms of peak values they are well below typical FOV limits in anti-tank guided missiles. Nevertheless, setting different parameters of the model (and disturbances) could lead to situation where LOS peak deflection is no longer acceptable for assumed requirements. Hence including presented internal disturbances in developed model and tuning controllers for that plant has potential to greatly improve gimbal's characteristics.

5. Conclusion

Presented results indicate that modelling gimbal seeker's internal disturbances such as: static imbalance, friction and cross coupling can significantly influence the quality of system responses when subjected to arbitrary inputs. This is especially important in the case of a system which controllers were initially tuned on model not considering these disturbances. Within this context, proposed, expanded unified model of disturbances is first step to significant increase of control systems disturbance rejection ability, what is critical from the point of view of system's accuracy.

As seen in figures 23 and 24, maximum line of sight's (LOS) deflection under circumstances of additional modelled disturbances changed by nearly 1100% and 160% respectively. Due to relatively high detection range requirements for anti-tank guided missiles, considering their restricted calibre, typical seeker's field of view (FOV) doesn't exceed 3 degrees [20]. Having in mind calculated increase of the LOS deflection, initial amplitude of as little as 0,15 degrees approximately could rise to unacceptable levels with the internal disturbances modelled and regulators not tuned accordingly. What is meant by "unacceptable" is losing track of a target, when it goes beyond image boundaries. Moreover, gimbal's deflections measured with encoders are used to drive missiles autopilot subsystems during flight, so without proper filters, change recorded in figures 23 and 24 could directly affect their movement and consequently miss distance.

Therefore, proposed unified model of disturbances acting upon gimbal seeker could greatly aid early design phase, giving engineers tool to describe modelled system more accurately. Anti-tank guided missiles are very costly to manufacture, but more importantly they are expensive in terms of development. Design that considers additional aspects of modelled physical phenomena helps in choosing correct control system's algorithms and also in tuning process.

AUTHOR

Radosław Nawrocki – Warsaw University of Technology, Pl. Politechniki 1, 00-661 Warsaw, Poland, e-mail: radoslaw.nawrocki.dokt@pw.edu.pl.

ACKNOWLEDGMENTS

This research was funded by PCO S.A. The author declares no conflict of interest.

REFERENCES

[1] N. R. Iyer, "Recent Advances in Antitank Guided Missile Systems", *Defence Science Journal*, vol. 45, no. 3, 1995, 187–197, 10.14429/dsj.45.4118.

[2] J. Osiecki and Z. Koruba, *Budowa, dynamika i nawigacja wybranych broni precyzyjnego rażenia*, Wydawnictwo Politechniki Świętokrzyskiej, 2006, (in Polish).

[3] N. Yu and J. Shang, "A Uniform Method of Mechanical Disturbance Torque Measurement and Reduction for the Seeker Gimbal in the Assembly Process", *Mathematical Problems in Engineering*, 2017, 187–197, 10.1155/2017/2179503.

[4] M. K. Masten, "Inertially stabilized platforms for optical imaging systems", *IEEE Control Systems Magazine*, vol. 28, no. 1, 2008, 47–64, 10.1109/MCS.2007.910201.

[5] M. Grzyb and K. Stefański, "The Control of Anti -Aircraft Missile Flight Path in Atmospheric Disturbances", *Maritime Technical Journal*, vol. 209, no. 2, 2017, 51–60, 10.5604/01.3001.0010.4066.

[6] G. Stroe and I.-C. Andrei, "Analysis Regarding the Effects of Atmospheric Turbulence on Aircraft Dynamics", *INCAS Bulletin*, vol. 8, no. 2, 2016, 123–132, 10.13111/2066-8201.2016.8.2.10.

[7] Ch.-L. Lin and Y.-H. Hsiao, "Adaptive feedforward control for disturbance torque rejection in seeker stabilizing loop", *IEEE Transactions on Control Systems Technology*, vol. 9, no. 1, 2001, 108–121, 10.1109/87.896752.

[8] T. F. Bridgland and J. S. Hinkel, "The minimum miss distance problem", *Proceedings of the American Mathematical Society*, vol. 18, no. 3, 1967, 457–464, 10.1090/S0002-9939-1967-0221355-8.

[9] "NATO - STANAG 4347 - Definition of Nominal Static Range Performance for Thermal Imaging Systems", NATO. https://standards.globalspec.com/std/518793/STANAG%204347. Accessed on: 2022-04-19.

[10] H. Olsson, K. J. Åström, C. Canudas de Wit, M. Gäfvert and P. Lischinsky, "Friction Models and Friction Compensation", *European Journal of Control*, vol. 4, no. 3, 1998, 176–195, 10.1016/S0947-3580(98)70113-X.

[11] T. Dumitriu, "Development of a Simulink® toolbox for friction control design and compensation", *The Annals of "Dunarea de Jos" University of Galati. Fascicle III, Electrotechnics, Electronics, Automatic Control, Informatics*, vol. 28, 2005.

[12] D. R. Otlowski, K. Wiener and B. A. Rathbun, "Mass properties factors in achieving stable imagery from a gimbal mounted camera". In: *Proceedings of SPIE 6946, Airborne Intelligence, Surveillance, Reconnaissance (ISR) Systems and Applications V*, 2008, 10.1117/12.778245.

[13] A. Toloei, M. Abdo, A. R. Vali and M. R. Arvan, "Research on gimbal seeker performance under variable operation conditions". In: *Proceedings of the 13th Iranian Aerospace Society Conference*, Tehran, Iran, 2014.

[14] C. Wang, R. Ning, J. Liu and T. Zhao, "Dynamic simulation and disturbance torque analyzing of motional cable harness based on Kirchhoff rod model", *Chinese Journal of Mechanical Engineering*, vol. 25, no. 2, 2012, 346–354, 10.3901/CJME.2012.02.346.

[15] J. J. Burgess, "Equations of Motion of a Submerged Cable with Bending Stiffness". In: *Proc. of the 11th International Conference on Offshore Mechanics & Arctic Engineering*, Calgary, Canada, June 1992.

[16] C. M. Ablow and S. Schechter, "Numerical simulation of undersea cable dynamics", *Ocean Engineering*, vol. 10, no. 6, 1983, 443–457, 10.1016/0029-8018(83)90046-X.

[17] B. Ekstrand, "Equations of motion for a two-axes gimbal system", *IEEE Transactions on Aerospace and Electronic Systems*, vol. 37, no. 3, 2001, 1083–1091, 10.1109/7.953259.

[18] M. Abdo, A. R. Vali, A. Toloei and M. R. Arvan, "Research on the Cross-Coupling of a Two Axes Gimbal System with Dynamic Unbalance", *International Journal of Advanced Robotic Systems*, vol. 10, no. 10, 2013, 10.5772/56963.

[19] S. Liu, T. Lu, T. Shang and Q. Xia, "Dynamic Modeling and Coupling Characteristic Analysis of Two-Axis Rate Gyro Seeker", *International Journal of Aerospace Engineering*, vol. 2018, 2018, 2022–01-14, 10.1155/2018/8513684.

[20] A. A. Shilin, "Обзор пассивных оптических ГСН для поражения наземных тактических целей Известия ТулГУ (Review of passive optical homing heads for destroying surface tactical targets)", *Technicheskiya Nauki*, vol. 7, 2014, 202–209, (in Russian).